



## RESEARCH ARTICLE

10.1002/2014JA019941

## Local time variations in Jupiter's magnetosphere-ionosphere coupling system

L. C. Ray<sup>1,2</sup>, N. A. Achilleos<sup>1</sup>, M. F. Vogt<sup>3</sup>, and J. N. Yates<sup>2</sup><sup>1</sup>Department of Physics and Astronomy, University College London, London, UK, <sup>2</sup>Space and Atmospheres Group, Imperial College London, London, UK, <sup>3</sup>Department of Physics and Astronomy, University of Leicester, Leicester, UK

## Key Points:

- Trends in auroral intensity with local time are reproduced by a simple 1-D model
- The strongest height-integrated currents flow through the dawn magnetosphere
- Future models must include azimuthal effects in MI coupling

## Correspondence to:

L. C. Ray,  
licia.ray@ucl.ac.uk

## Citation:

Ray, L. C., N. A. Achilleos, M. F. Vogt, and J. N. Yates (2014), Local time variations in Jupiter's magnetosphere-ionosphere coupling system, *J. Geophys. Res. Space Physics*, 119, 4740–4751, doi:10.1002/2014JA019941.

Received 5 MAR 2014

Accepted 2 JUN 2014

Accepted article online 6 JUN 2014

Published online 27 JUN 2014

**Abstract** The ionization of neutral material ejected by Jupiter's volcanically active moon, Io, results in a plasma disc that extends from Io's orbit out through the Jovian magnetosphere. This magnetospheric plasma is coupled to the planetary ionosphere via currents which flow along the magnetic field. Inside of  $\sim 40 R_J$ , these currents transfer angular momentum from the planet to the magnetospheric plasma, in an attempt to keep the plasma rigidly corotating with the planet. Jupiter's main auroral emission is a signature of this current system. To date, one-dimensional models of Jupiter's magnetosphere-ionosphere (M-I) coupling have either assumed a dipole field or used a field description appropriate to the postmidnight region of the Jovian magnetosphere. Vogt et al. (2011) described the variation of the N-S component of the magnetic field in the center of the current sheet,  $B_N$ , with local time and radius. We apply a 1-D model of Jupiter's M-I current system every hour in local time using a modified description of the Vogt et al. (2011) magnetic field to investigate how local time variations in the magnetosphere affect the auroral currents and plasma angular velocity. Our model predicts the strongest aurora at dawn, with a minimum in the auroral currents existing from noon through dusk. This is a few hours duskward of the discontinuity predicted by Radioti et al. (2008). While our model predictions are consistent with some of the observations, future MI coupling models must account for the azimuthal bendback in the magnetic field.

## 1. Introduction

Jupiter's main auroral oval is the most persistent auroral emission in the solar system, driven by corotation enforcement currents that couple the planetary ionosphere to the middle magnetospheric plasma. The main auroral emission has been observed extensively at X-ray, ultraviolet (UV), infrared (IR), and visible wavelengths, using Chandra, X-MM Newton, the Hubble Space Telescope (HST), Cassini Ultraviolet Imaging Spectrograph instrument, ground-based telescopes, and the Galileo solid state imaging system [e.g., Clarke et al., 1998; Vasavada et al., 1999; Stallard et al., 2001; Grodent et al., 2003; Melin et al., 2006; Radioti et al., 2008; Branduardi-Raymont et al., 2008; Nichols et al., 2009; Gérard et al., 2013]. Fixed in System III, Jupiter's longitude system, and therefore rotating with the planet, the main emission rotates in and out of sight for an Earth-based observer because of the offset, tilted dipole nature of the Jovian magnetic field. The latitudinal extent of the UV main auroral emission is on the order of  $\sim 1\text{--}3^\circ$  and its Jovicentric location is steady, with variations of only  $\sim 3^\circ$  that are possibly driven by changes in solar wind and/or internal magnetospheric plasma conditions [Grodent et al., 2008a]. Gustin et al. [2004] found that the emission was excited by precipitating electrons with energies of  $\sim 30\text{--}200$  keV and associated precipitating electron energy fluxes of  $\sim 3\text{--}200$  mW m<sup>-2</sup>. Radioti et al. [2008] discovered a persistent fading in the postdawn/prenoon sector, with a mean location of 1000 LT [Radioti et al., 2008], coincident with the location of reduced radial currents [Khurana, 2001]. In addition to these "typical" characteristics, there are also dawn storms during which the intensity of the dawn oval is associated with precipitating electron fluxes of  $\sim 100$  mW m<sup>-2</sup> [Gustin et al., 2006]. The dusk region emission, which is broader, less discrete, and far less regular in morphology than the dawn emission, will occasionally exhibit multiple arcs [Nichols et al., 2009].

Jupiter's main auroral emission is created by precipitating electrons from the upward current system that transfers angular momentum from the planetary atmosphere to the magnetosphere. As magnetospheric plasma moves radially outward, the tendency to conserve angular momentum dictates that it slows down. The plasma is frozen-in to the planetary magnetic field, the footprints of which are rooted in the planet. Therefore, as the plasma slows from corotation, the field becomes swept back azimuthally. Any bendback in the field is simultaneously supported by radial currents. These currents travel radially outward in the

This is an open access article under the terms of the Creative Commons Attribution License, which permits use, distribution and reproduction in any medium, provided the original work is properly cited.

magnetosphere and are closed by field-aligned currents flowing between the magnetospheric plasmasheet and the planetary ionosphere, and latitudinal currents in the ionosphere. The radial currents exert a  $\mathbf{J} \times \mathbf{B}$  force on the plasma in the sense of corotation. Hill [1979] was the first to describe this current system, equating the magnetospheric and ionospheric torques and determining the angular velocity of the magnetospheric plasma. His analysis assumed a dipole planetary field, constant ionospheric Pedersen conductance, equipotential field lines, and a corotating thermosphere. The currents transferring angular momentum were linked to Jupiter's main auroral emission by concurrent studies in 2001 [Hill, 2001; Cowley and Bunce, 2001], and henceforth, we will call them auroral currents.

A number of the simplifying assumptions in Hill [1979] have since been further investigated, both analytically and numerically, including the slowing of the thermosphere due to ion-neutral collisions and inefficient transfer of angular momentum from the deep interior to upper atmosphere (analytical: Huang and Hill [1989] and numerical: Smith and Aylward [2009]; Tao et al. [2009]; Yates et al. [2012, 2014]) (L. C. Ray et al., Including field-aligned potentials in the coupling between Jupiter's thermosphere, ionosphere, and magnetosphere, submitted to *Planetary and Space Sciences*, 2014); nondipolar field geometries (analytical: Pontius [1997] and numerical: Cowley and Bunce [2001, 2003]; Nichols [2011]); variable Pedersen conductances (numerical: Nichols and Cowley [2004]; Tao et al. [2010]; Ray et al. [2010]); and the rotational decoupling allowed by field-aligned potentials (numerical: Nichols and Cowley [2005]; Ray et al. [2010, 2012, also submitted manuscript, 2014]). The numerical models use a 1-D description of the auroral current system to couple the ionosphere to the magnetosphere, mapping electric fields and currents between magnetically conjugate regions using a prescribed magnetic field geometry. This 1-D description simplifies the treatment of the magnetosphere and ionosphere, approximating both regions as thin slabs. A numerical multidimensional approach to M-I coupling at Jupiter that would employ more physically realistic descriptions of the magnetosphere and ionosphere is currently impractical. Resolving the high-latitude regions of the planetary magnetosphere, where the Alfvén velocity,  $v_A$ , approaches the speed of light, is computationally intensive and prohibitive as the Courant condition requires a time step of  $\delta t < \frac{\delta x}{v_A}$ . Magnetohydrodynamic (MHD) models of the outer planets adjust for this by specifying a conducting sphere of several planetary radii as the inner boundary condition for their simulations. For example, Walker and Ogino [2003] used an MHD model to explore the currents in the Jovian system using an inner boundary of  $15 R_J$ . Chané et al. [2013] provides an excellent review of the inner boundary conditions used at Jupiter for MHD simulations. Their work pushed the inner boundary into  $8 R_J$ ; however, this is still outside the orbit of Io and its plasma torus, which supplies the plasma mass in the Jovian magnetosphere.

Because of the  $9.6^\circ$  tilt of Jupiter's dipole magnetic field relative to the planetary rotation axis, dipole offset from the center of the planet, and the nondipolar multiples of the global magnetic field, the northern auroral emissions are more easily observed than those in the southern hemisphere. Additionally, observations at certain central meridional longitudes,  $\sim 110^\circ$ – $260^\circ$ , are preferable because of the dipole tilt direction [Grodent et al., 2003, Figure 8]. Therefore, it can be difficult to separate which variations in the auroral emission are caused by local time asymmetries in the magnetosphere as opposed to variations in the internal planetary magnetic field.

There are a number of observed local time asymmetries in Jupiter's magnetosphere. Outside of  $\sim 20 R_J$ , magnetic perturbations from azimuthal currents rival, and with increasing radial distance dominate, the magnitude of the magnetic field signature owing to the internal field [Khurana et al., 2004]. Khurana [2001] used Galileo magnetometer data to find local time variations in the azimuthal currents, with the magnitude being larger on the nightside than dayside. Local time variations are also present in the radial currents, with stronger height-integrated currents in the predawn region than premidnight. Kivelson and Khurana [2002] found that the plasmasheet is thicker at dusk than at midnight through dawn. Local time asymmetries have also been observed in the plasma flows. Using the Galileo energetic particle detector (EPD), Krupp et al. [2001] measured faster azimuthal flows in the dawn sector than through dusk. While present at radial distances as close to Jupiter as  $\sim 15 R_J$ , the local time asymmetries in the plasma flow were most pronounced outside of  $\sim 30 R_J$ .

Vogt et al. [2011] investigated how local time variations in the magnetic field affected the mapping of magnetospheric locations to their magnetically conjugate counterparts in the ionosphere. To do this, they determined the local time variation of the component of the magnetic field normal to the current sheet,  $B_N$ , using magnetometer data to identify current sheet crossings. They found a systematic variation in  $B_N$

**Table 1.** Coefficients for the Normal Component of the Magnetospheric Magnetic Field<sup>a</sup>

Coefficient	Value
$\alpha$	-5.893E4
$\beta$	$\frac{2\pi}{15}$
$\gamma$	8.602E4
A <sup>a</sup>	1.030E6
B <sup>a</sup>	-3.756
C <sup>a</sup>	-0.120
D <sup>a</sup>	3.562
E <sup>a</sup>	3.797
F <sup>a</sup>	-4.612
G <sup>a</sup>	0.825
H <sup>a</sup>	0.606
I <sup>a</sup>	0.473
J <sup>a</sup>	0.847
K <sup>a</sup>	0.913

<sup>a</sup>Coefficients defined in Vogt *et al.* [2011].

as a function of radius and local time, with  $B_N$  stronger in the noon through dusk sectors than through midnight and dawn. Magnetically conjugate locations in the ionosphere and magnetosphere were then determined by mapping regions of equivalent magnetic flux. Vogt *et al.* [2011] accounted for the bendback in the magnetospheric magnetic field by shifting the azimuthal location in the current sheet according to a fit to magnetometer data presented by Khurana and Schwarzl [2005]. According to the model of Vogt *et al.* [2011], at dawn the main auroral emission maps to an equatorial location of  $\sim 15\text{--}30 R_J$  (Jovian radii,  $1 R_J = 7.1492 \times 10^7$  m), while at postnoon the mapping location is farther out in the magnetosphere,  $\sim 50\text{--}60 R_J$ .

Local time asymmetries in Jupiter's magnetic field are most pronounced outside of  $\sim 20 R_J$ . These asymmetries affect the latitudinal extent of flux mapping for a given equatorial range in the magnetosphere. We use the Vogt *et al.* [2011] description of the component of the magnetospheric magnetic field normal to the current sheet,  $B_N$ , modified to extend into  $5 R_J$ , coupled with a Hill-like 1-D model of the auroral currents, constructed under simplified assumptions—constant ionospheric Pedersen conductance, equipotential field lines, and a dipole field at Jupiter—to investigate how variations in the magnetospheric magnetic field structure affect the magnitude and position of the auroral currents with local time. Starting with a corotational plasma at  $5 R_J$ , we evolve the electrical currents and plasma angular velocities in the middle mag-

netosphere. In order to build a map of the currents and velocities with radius and local time, the 1-D model is applied every hour or, equivalently, every  $15^\circ$ , in local time. In this study, we derive an analytic expression for the magnetic flux function at the planet as a function of latitude and local time assuming a dipole field. This simplifying assumption, which ignores the azimuthal bendback in the magnetospheric field and higher-order moments at the planet, allows us to determine the suitability of employing 1-D slices that vary in local time in future magnetosphere-ionosphere-thermosphere coupling studies.

The paper is structured as follows: in section 2 we describe the model used to calculate the auroral currents. Section 3 describes our results and compares them with descriptions of previously reported auroral observations and in situ measurements, and previous modeling efforts. Finally, we conclude in section 4.

## 2. Theoretical Background

### 2.1. Magnetic Field Model and Flux Function

The Vogt *et al.* [2011] field description was derived using data outside of  $20 R_J$ . However, in this study we are interested in the motion of plasma outward from the Io torus. Therefore, we have modified the original Vogt *et al.* [2011] description to include an attenuated dipole such that the N-S component of the field, from the inner boundary at  $5 R_J$  to an outer boundary of  $100 R_J$  is as follows:

$$B_N(r, \phi) = X \left( \frac{1}{r} \right)^3 e^{-\left( \frac{r}{r_0} \right)^{5/2}} + A r^Y + Z e^{-r/150} \quad (1)$$

where  $r$  is the radial distance in  $R_J$  and  $r_0 = 14.501 R_J$ . For simplicity, the local time dependence is quantified by the variables  $X$ ,  $Y$ , and  $Z$

$$X = \alpha \cos(\phi - \beta) + \gamma \quad (2)$$

$$Y = B + C \cos(\phi - D) \quad (3)$$

$$Z = E + F \cos(\phi - G) + H \cos(2(\phi - I)) + J \cos(3(\phi - K)) \quad (4)$$

where  $\phi$  is the local time, measured from midnight in radians, and the coefficients  $\alpha\text{--}\gamma$  and A-K [Vogt *et al.*, 2011] are defined in Table 1. The first term on the right-hand side (RHS) of equation (1) is the attenuated dipole while the second and third terms on the RHS are the RHS of equation (1) from Vogt *et al.* [2011]. The coefficient  $X$  for the attenuated dipole term ensures that the magnitude of the field function matches that of a dipole field at  $5 R_J$  for all local times. Figure 1 (top) shows  $B_N(r, \phi)$  as a function of radial distance from 5 to  $100 R_J$ . For all local times, the field is similar until  $\sim 15 R_J$ . Figure 1 (middle) displays  $B_N(r, \phi)$  for all local times

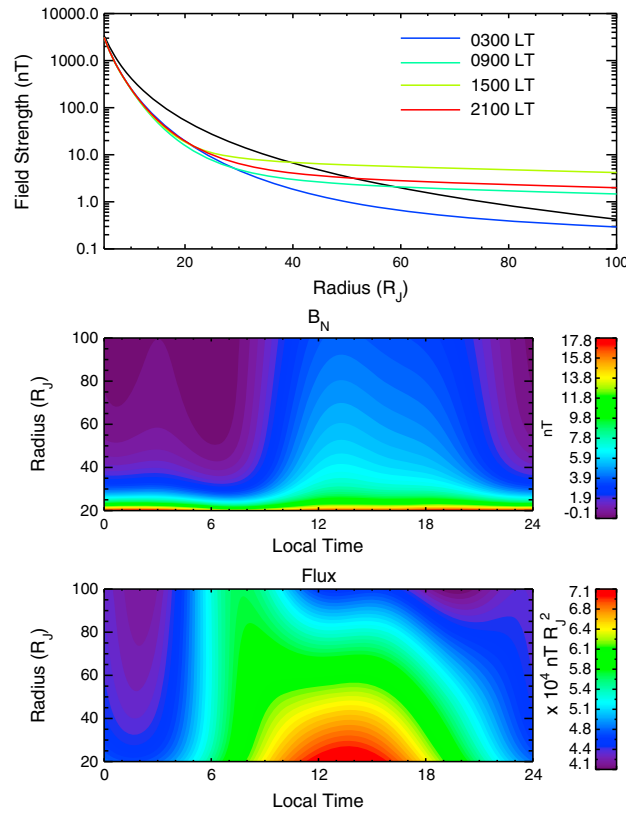


**Figure 1.** The magnitude of the N-S component of the magnetic field, (top)  $B_N$  as a function of radius at 0300 LT (blue), 0900 LT (green), 1500 LT (mustard), and 2100 LT (red). The black line shows the magnitude of a dipole. (middle) The full description of  $B_N$  with local time and radius outside of  $20 R_J$  with (bottom) the corresponding flux function,  $F_e$ .

for equatorial distances larger than  $20 R_J$ . The dayside magnetopause location is bimodal, with the most probable standoff distances at  $63 R_J$  and  $92 R_J$ . Therefore, while the *Vogt et al.* [2011] model is valid to distances of  $150 R_J$ , we select an outer boundary of  $100 R_J$  for this study as the coupling between the ionosphere and magnetosphere near the boundary is not well understood.

To map magnetically conjugate regions of the magnetosphere and ionosphere, it is necessary to derive a flux function. We assume that the magnetic field at the planetary atmosphere can be approximated as a dipole in order to investigate the effects of local time on the auroral currents, independent of the longitudinal and latitudinal variations in the planetary magnetic field that are due to higher-order multiples. We also ignore the bendback (azimuthal component) of the magnetospheric magnetic field, so that a given ionospheric longitude corresponds to a radial slice in the magnetosphere. Under this assumption, we can equate the magnetospheric and ionospheric fluxes per unit azimuth

$$F_i(\theta_i) = F_e(r) \quad (5)$$

where  $\theta_i$  is planetary colatitude, and the magnetic flux per unit azimuth threading the ionosphere at each local time between colatitudes zero and  $\theta_i$  is simply

$$F_i(\theta_i) = B_J R_J^2 \sin^2 \theta_i \quad (6)$$

where  $B_J = 4.264 \times 10^5$  nT is Jupiter's surface equatorial field strength. The flux per unit azimuth threading the equatorial plane is more complicated and given by

$$F_e(r, \phi) = \int_r^\infty r' B_N(r', \phi) dr' \quad (7)$$

Outside of the inner boundary of  $5 R_J$  the flux function is therefore

$$F_e(r, \phi) = F_\infty(\phi) + \frac{X}{2.5r_0} \Gamma \left[ -\frac{2}{5}, \left( \frac{r}{r_0} \right)^{5/2} \right] + \frac{A}{Y+2} r^{Y+2} - 150(r+150)e^{-r/150} Z \quad (8)$$

where  $F_\infty(\phi)$  is the value of the magnetic flux from the edge of the outer boundary at  $100 R_J$  to infinity:

$$F_\infty(\phi) = \frac{1}{5} B_J R_J^2 + \frac{X}{2.5r_0} \Gamma \left[ -\frac{2}{5}, \left( \frac{5}{r_0} \right)^{5/2} \right] + \frac{A}{Y+2} 5^{Y+2} - 2.24878 \times 10^4 \times Z \quad (9)$$

The flux function is shown in Figure 1 (bottom).

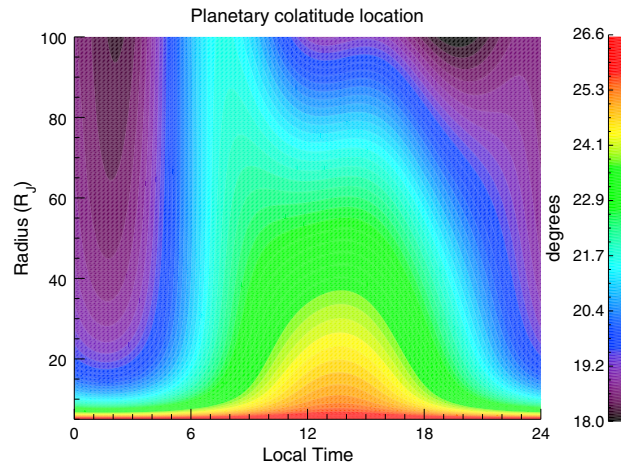


**Figure 2.** The magnetically conjugate ionospheric location for a point in the magnetospheric equatorial plane as a function of local time.

The ionospheric and equatorial fluxes are then equated, hence, the ionospheric colatitude corresponding to a magnetospheric equatorial location as a function of radial distance and local time,  $\theta_i(r, \phi)$ , can be given by

$$\theta_i(r, \phi) = \sin^{-1} \sqrt{\frac{F_e(r, \phi)}{B_j R_j^2}} \quad (10)$$

The magnetically conjugate colatitude at the ionosphere for a given location in the equatorial plane as a function of local time and radius, from 5 to 100  $R_j$ , is shown in Figure 2. Radial slices from 15–100  $R_j$  in the midnight through postmidnight sector are magnetically conjugate with a narrower band of colatitudes, spanning  $\sim 2^\circ$ , than equivalent

radial slices in the noon through dusk regions, which span  $\sim 5^\circ$  in colatitude. While the inner boundary of 5  $R_j$  in the equatorial plane maps to an ionospheric colatitude of  $26.6^\circ$ , regardless of local time, variations in the flux function lead to noticeable local time asymmetries in the ionospheric colatitude for radial distances  $\geq 7 R_j$ .

The perpendicular distance from the spin axis to the ionospheric footprint at the surface of the planet, magnetically conjugate with a magnetospheric equatorial position of  $(r, \phi)$ , is

$$s(r, \phi) = R_j \sqrt{\frac{F_e(r, \phi)}{B_j}} \quad (11)$$

such that the mapping between the ionosphere and magnetosphere  $\alpha$  is simply provided using conservation of magnetic flux:

$$\alpha(r, \phi) = \frac{B_j s(r, \phi)}{B_N(r, \phi) r} = \frac{dr}{R_j d\theta_i} \quad (12)$$

where  $B_j$  is the magnetic field strength at the ionospheric end of the flux tube, which we fix in this analysis to be  $2B_j$ .

### 2.2. Auroral Currents and Angular Velocities

Having derived a method to relate the magnetospheric and ionospheric regions, the determination of the auroral currents and plasma angular velocity is straightforward. Following Hill [1979], the torque balance between the ionospheric and magnetospheric plasma is represented as

$$\dot{M} \frac{d}{dr} (r^2 \Omega_M(r, \phi)) = 2\pi r^2 K_M(r, \phi) B_N(r, \phi) \quad (13)$$

where  $\dot{M}$  is the radial mass transport rate in  $\text{kg s}^{-1}$ ,  $\Omega_M(r, \phi)$  is the angular velocity of the magnetospheric plasma, and  $K_M(r, \phi)$  is the height-integrated radial current in  $\text{A m}^{-1}$ . For ease of the calculation, we introduce the plasma's deviation from corotation with Jupiter,  $\omega(r, \phi)$ , such that  $\Omega_M(r, \phi) = \Omega_j + \omega(r, \phi)$  where  $\Omega_j$  is Jupiter's angular velocity ( $1.7735 \times 10^{-4} \text{ rad s}^{-1}$ ).

Any deviation in corotation produces an electric field,  $E_M$ , of magnitude

$$E_M(r, \phi) = \omega(r, \phi) B_N(r, \phi) r \quad (14)$$

at the equatorial plane, which, assuming that the magnetic field lines are equipotentials, corresponds to a latitudinal ionospheric electric field,  $E_I$ , given by:

$$E_I(r, \phi) = \alpha E_M(r, \phi) \quad (15)$$

For an assumed ionospheric Pedersen conductance, the ionospheric height-integrated current,  $K_i$ , is thus given by Ohm's law as

$$K_i(r, \phi) = \Sigma_p E_i(r, \phi) \quad (16)$$

This can be related to a magnetospheric height-integrated current density,  $K_M(r, \phi)$ , such that

$$K_M(r, \phi) = -2K_i(r, \phi) \frac{r}{R} \quad (17)$$

where the negative sign reflects the change in the direction of current from equatorward at the ionosphere to radially outward in the magnetospheric equatorial plane, assuming a 1-D model. It may seem odd to describe ionospheric parameters as a function of equatorial radial distance; however, this representation reflects the 1-D nature of the model, and all points in the magnetosphere can be related to a magnetically conjugate ionospheric location through equation (10).

Equations (13)–(17) are numerically solved using an Euler predictor-corrector scheme as a function of radius for each local time. The solutions are initialized with a corotating plasma ( $\omega(5, \phi) = 0$ ). Following the evaluation of equations (13)–(17), it is trivial to evaluate the field-aligned current density using current continuity,  $\nabla \cdot \mathbf{j} = 0$ . The magnetospheric field-aligned current density,  $j_{\parallel M}$  is

$$j_{\parallel M}(r, \phi) = \frac{1}{r} \frac{d}{dr} \left( \frac{rK_M(r)}{2} \right) \quad (18)$$

with the ionospheric current density,  $j_{\parallel i}$ , determined by scaling to the magnetic mirror ratio between the ionosphere and equatorial plane,  $R_M = B_i/B_M$ :

$$j_{\parallel i} = R_M j_{\parallel M} \quad (19)$$

In this analysis, to isolate the effects of local time variations in the magnetic field, we ignore the modification of the Pedersen conductance and development of field-aligned potentials for values of the ionospheric current density greater than the local thermal field-aligned current density,  $j_{\text{mth}}$

$$j_{\text{mth}} = n_e e \sqrt{T_e / 2\pi m_e} \quad (20)$$

where  $m_e = 9.11 \times 10^{-31}$  kg is the electron mass,  $e = 1.6022 \times 10^{-19}$  C is the fundamental charge,  $n_e$  is the local electron density, and  $T_e$  is the energy of the thermal electron.

### 3. Results and Discussion

For complete coverage in local time, we apply our model every 15° in inertial longitude or, equivalently, every hour in local time, and at each local time span, the 5 to 100  $R_j$  range of equatorial distances. *Delamere et al.* [2005] used a physical chemistry model to determine that, after charge exchange, 250–600 kg  $s^{-1}$  of plasma is available for radial transport, from a neutral source rate of 500–1200 kg  $s^{-1}$ . *Millward et al.* [2002] found the Pedersen conductance to vary between 0.1 mho and 8 mho with precipitating particle energy and particle flux. In order to clearly understand the effect of local time variations in the N-S component of the equatorial magnetic field, we use canonical values for the radial mass transport rate ( $\dot{M} = 1000$  kg  $s^{-1}$ ) and the ionospheric Pedersen conductance ( $\Sigma_p = 0.1$  mho) for all local times. It should be noted that the flux function at 0600 LT is nonmonotonic because of the functional form of  $B_N$ . Therefore, for this location only, we average the runs at 0500 LT and 0700 LT to determine the plasma angular velocity, electric fields, and current intensities.

Figure 3 shows the magnetospheric plasma angular velocity as a function of local time. Inside of  $\sim 20 R_j$ , the angular velocities are largely independent of local time and the plasma is near corotational. Outside of  $\sim 20 R_j$ , there are strong variations with local time. From 0900 LT to 2000 LT, the plasma angular velocity seldom falls below 0.5  $\Omega_j$ . However, from 2300 LT to 0800 LT, the plasma velocity continues to fall outside of  $\sim 40 R_j$ , reaching velocities as low as 0.1  $\Omega_j$ . The stark difference in the plasma flow speeds can be easily explained by the variations in  $B_N$ . As shown in Figure 1, the magnitude of  $B_N$  is larger in the noon through dusk region. Therefore, less radial current is required to exert a similar  $\mathbf{J} \times \mathbf{B}$  in the noon/dusk region than in the postmidnight/dawn region.

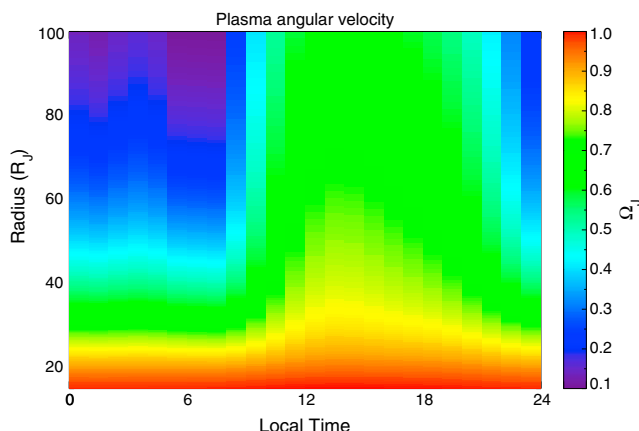


**Figure 3.** The angular velocity of the magnetospheric plasma as a function of local time and radius normalized to corotation with Jupiter.

torque balance in the azimuthally symmetric approximation and therefore excludes azimuthal currents. At Jupiter, Walker and Ogino [2003] found that the azimuthal ring current closed through outward radial and field-aligned currents on the dawn side, but through inward pointing radial currents in the dusk sector, consistent with the radial currents measured by Galileo [Khurana, 2001]. This closure of azimuthal currents acts to enforce the corotation currents at dawn and act against them at dusk. A more complete description of the system, including the continuity and momentum equations such as in the MHD approach, might help reconcile the difference between the modeled and observed angular velocities. However, how to couple a more complete, multidimensional approach to the atmosphere remains an open research topic.

Figure 4 displays the height-integrated radial current, in  $MA R_J^{-1}$ , in the magnetosphere at each sampled local time. In the noon/dusk regions, the maximum height-integrated radial current, found at  $\sim 30 R_J$ , is less than half the maximum height-integrated radial current in the dawn sector from 0500 to 0800 LT, which is located at  $\sim 40\text{--}50 R_J$ . The region of relatively low height-integrated radial currents from 1200 to 1800 LT overlaps with where Khurana [2001] found a return current region in the Galileo magnetometer data from  $\sim 0900$  to 1300 LT. We can compare the height-integrated radial currents predicted in this model to those derived from Galileo data and shown in Figure 12 of Khurana [2001]. Similar to the Galileo currents, the height-integrated radial currents calculated in this study are roughly uniform with local time out to  $\sim 20 R_J$ . Outside of  $25 R_J$ , Khurana [2001] found that the height-integrated radial currents are strongest from 0300 LT to 0600 LT, weakening through noon. This is a shift toward dawn from the currents predicted by our model and may be explained by the lack of field bendback in our field description. At all radial distances, our study underestimates the magnitude of the height-integrated radial currents by a factor of  $\sim 2$  from 30 to  $50 R_J$ , and an order of magnitude in the outer and inner magnetosphere.

With such large variations in the height-integrated radial current as a function of local time, it is not surprising that both the intensity and location of the auroral currents are also modulated with local time as seen in Figure 5. As we are interested in the likely location of the aurora, the ionospheric current density is only

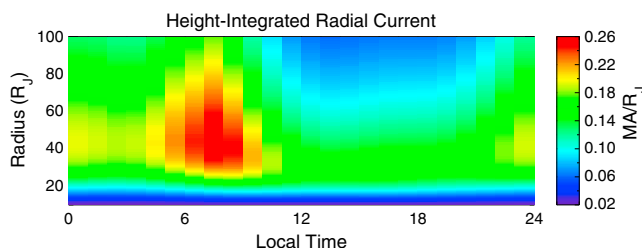


**Figure 4.** Height-integrated radial current, in  $MA R_J^{-1}$ , as a function of local time and radius.

The local time variation in the predicted angular velocities is opposite to the trend measured by Galileo in the energetic particle data [Krupp et al., 2001]. Krupp et al. [2001] found faster flows in the dawn sector than near dusk, where the flows were subcorotational from 20% to 80% of corotation. The noon-dusk sector was not adequately sampled. The EPD observations are consistent with a steady state system in which the flux transport ( $\int \Omega_M(r, \phi) B_N(r, \phi) r^2 dr$ ) is a constant with local time; the plasma angular velocities predicted by our model are not consistent with such a picture. This is because our 1-D model is built from an argument of

shown where it is larger than the electron thermal current density,  $j_{mth}$ . We assume an electron density of  $n_e = 0.01 \text{ cm}^{-3}$  and an electron temperature of 2.5 keV [Scudder et al., 1981], yielding  $j_{mth} = 0.013 \mu A \text{ m}^{-2}$ . When the condition  $j_{||} > j_{mth}$  is met, field-aligned potentials will develop to boost the electron distribution into the loss cone, increasing the field-aligned current and accelerating electrons into the planetary

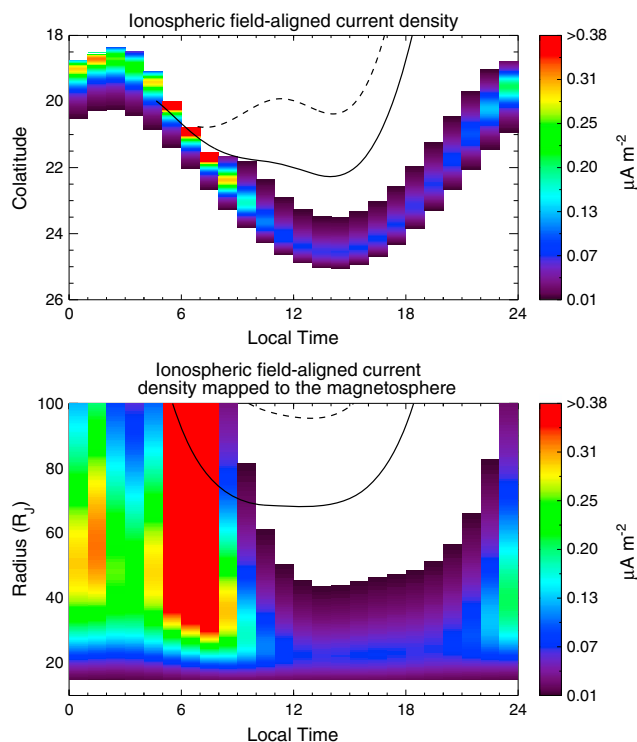


**Figure 5.** (top) The intensity and location of the ionospheric field-aligned current density as a function of colatitude and local time. The compressed and extended magnetopause boundary locations out to 120  $R_J$  are shown with solid and dashed lines, respectively. (bottom) The magnetically conjugate magnetospheric locations for the auroral currents. Empty regions are either outside the magnetosphere or represent regions where the ionospheric field-aligned current density is less than the thermal electron current density.

ionosphere. Therefore, auroral emissions are expected to coincide with the locations where  $j_{||} \gg j_{mth}$ . Consistent with the height-integrated radial current profiles, the most intense auroral currents occur between 0500 LT and 0700 LT. At these locations, the maximum current density exceeds that shown on Figure 5, reaching  $\sim 1.1 \mu A m^{-2}$ . Such large field-aligned current densities might be unrealistic, depending on the nature of the auroral acceleration region. Owing to the centrifugal confinement of the magnetospheric plasma and the gravitational confinement of the ionospheric plasma, the top of the auroral acceleration region is predicted to exist at radial distances of  $\sim 2-3 R_J$  Jovicentric, coincident with the minimum in the sums of the gravitational and centrifugal potentials [Su *et al.*, 2003]. If the acceleration region exists at high magnetic latitudes, as indicated by Vlasov simulations of the Jovian system [Ray *et al.*, 2009], the field-aligned current density would saturate before reaching such large magnitudes, i.e., the entire electron distribution would be boosted into the loss cone, thus preventing further increases in  $j_{||}$ .

We fix the outer boundary of our model at 100  $R_J$  for all local times. However, in the physical system, the shape of the magnetosphere is not uniform, varying with local time and solar wind conditions. The nominal compressed and expanded magnetopause boundaries, out to 120  $R_J$ , are shown in Figure 5 with solid and dashed lines, respectively [Joy *et al.*, 2002]. In both magnetospheric configurations, the dawn sector auroral currents run up to the magnetospheric boundary. Particularly from 0500 LT to 0700 LT, the poleward boundary of the currents coincides with the magnetopause boundary, which would give rise to sharp changes in the auroral currents. This would possibly lead to the narrow, discrete arcs seen in the UV auroral observations [Grodent *et al.*, 2003; Clarke *et al.*, 2004; Nichols *et al.*, 2009].

In contrast, the modeled noon/dusk auroral currents are faint and would be expected to produce dim auroral emissions, if any. While the small magnitude of the auroral currents is consistent with the assumed field geometry, it is inconsistent with auroral observations, which show nearly continuous, bright emission through all observable local times with the exception of the prenoon discontinuity [Radioti *et al.*, 2008]. The weakest auroral currents in the model exist postnoon, near 1400 LT. This is duskward of where Radioti *et al.* [2008] reported a persistent discontinuity in the main emission with a mean location of 1000 LT and a mean width of  $\sim 35^\circ$ , or 2 h in local time. This discrepancy is consistent with the lag in the predicted height-integrated currents relative to those inferred by Galileo magnetometer data.

Through the noon/dusk sector, the poleward boundary is separated by as much as  $3^\circ$  from the magnetopause boundary. The dusk sector is often associated with broad (in latitude) emission [Grodent *et al.*, 2003]; however, while much of this is spreading because of nondipolar components in the northern planetary magnetic field located from  $110^\circ$  to  $150^\circ \lambda_{III}$ , some may be driven by local time variations in the magnetosphere.

Between 1400 LT and 0200 LT, there is a difference of  $5^\circ$  colatitude in the location of the currents. The colatitude versus local time dependence of the peak auroral current follows a sinusoidal function, which is unsurprising as we do not account for the azimuthal bendback of the magnetic field in our model since we are testing the validity of applying a 1-D model to different local time sectors in Jupiter's magnetosphere. Therefore, radial slices through the magnetosphere map to magnetically conjugate ionospheric latitudes at the same longitude, rather than drifting in ionospheric longitude. Measurements of Jupiter's magnetosphere show that, outside of  $40 R_J$ , there is a non-negligible azimuthal component to the magnetic field [Khurana, 2001; Khurana and Schwarzl, 2005]. In the dawn sector, the magnetic field is strongly swept back, while through dusk the field is swept forward in the rotational direction. Allowing for shifts in the azimuthal ionospheric mapping location for a radial magnetospheric slice may "smear" out the modeled latitudinal variation and is a project for future work.

Jupiter's northern aurora is the most easily observed because of the tilted, offset, nondipolar field, with a magnetic anomaly existing in the northern hemisphere [Grodent *et al.*, 2008b]. Because of this, it is difficult to cleanly determine the average latitudinal span of the oval. Grodent *et al.* [2008a] found that the location of the main auroral emission varies by up to  $\sim 3^\circ$  in latitude with changing solar wind and/or internal plasma conditions. Estimates of the auroral oval width from HST images yield a typical latitudinal extent, from the center of the oval to the emission, of  $\sim 15^\circ$  [Clarke *et al.*, 1998; Grodent *et al.*, 2003, 2008a; Nichols *et al.*, 2009], with the northern oval being slightly larger than the southern emission [Gérard *et al.*, 2013] because of the offset of the dipole toward the north. The mean predicted location of the aurora in our model is  $\sim 22^\circ$  colatitude. Thus, qualitatively, our model predicts a wider auroral oval than that observed. Including an appropriate description of the surface field might reconcile the model and observations, although it may also mask out the effect of local time variations on the width and intensity of the auroral, which is the aim of this exercise. Vogt *et al.* [2011] changed the orientation of the dipole with subsolar longitude when performing an equivalent flux mapping study between the magnetosphere and ionosphere. To account for the bendback of the planetary field, they used a nominal bendback from a fit to the Galileo data from Khurana and Schwarzl [2005]. Vogt *et al.* [2011] determined that equivalent radial regions in the dusk sector map to broader latitudinal bands than in the dawn sector for all subsolar longitudes; however, variations in the auroral width exist with subsolar longitude.

Figure 5 (bottom) presents that the ionospheric field-aligned current, where  $j_{||i} > j_{mth}$ , is projected onto its magnetically conjugate magnetospheric location as a function of the equatorial radius and local time. Unsurprisingly, the inner boundary of the auroral currents is fairly constant with local time, around  $\sim 15 R_J$ . However, the outer boundary of the current system varies strongly with local time. Through midnight and dawn, the radial extent of the auroral currents reaches the outer boundary of the model, making it difficult to relate magnetospheric observations to features in the aurora. In the noon/dusk sector, the modeled auroral currents only extend to  $\sim 50 R_J$ . This is consistent with observations of the dusk aurora, where emission poleward of the main emission exhibits time variability and is hence unrelated to corotation enforcement currents [Nichols *et al.*, 2009]. The driving mechanism for aurora poleward of the main auroral emission is still not well understood. Additionally, variations in the observed auroral emission with local time may reflect changes in the magnetospheric plasma disc. For example, Kivelson and Southwood [2005] postulated that as magnetospheric plasma rotates and moves radially outward, from noon through dusk in the outer magnetosphere, it gains parallel energy as it moves out across the centrifugal potential. This process results in a thick plasmashet, the thickness of which is reflected in the magnitude of  $B_N$ , but we do not include changes in the plasma population with local time. Implementing local time variations in the radial mass transport rate is an avenue for future work.

Two other simplifying assumptions are the constant Pedersen conductance and lack of thermospheric feedback in the model. Enhancements in the Pedersen conductance increase the ionospheric currents, and hence increase the transfer of angular momentum from the planet to the surrounding magnetospheric plasma. Including the enhancement of  $\Sigma_p$  would likely increase the angular velocity of the magnetospheric plasma and the intensity of the auroral currents, as in the study by Nichols and Cowley [2004]. Just as the magnetosphere experiences a force accelerating the plasma toward corotation, the ionospheric plasma experiences an equal and opposite force, slowing it down. Through ion-neutral collisions, this persistent anti-corotational force will decelerate the neutral atmosphere under the main auroral oval, provided the transfer of angular momentum from the deep atmosphere to the thermosphere is inefficient, thereby limiting the angular momentum that is available to be transferred out to the magnetospheric plasma.

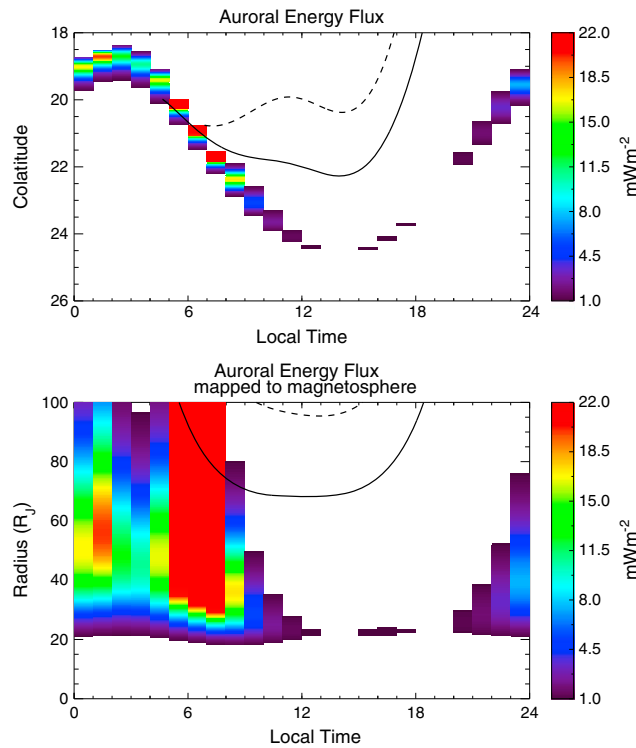


**Figure 6.** (top) An estimate of the precipitating auroral energy flux ( $> 1 \text{ mW m}^{-2}$ ) as a function of colatitude and local time. The compressed and extended magnetopause boundary locations out to  $120 R_J$  are shown with solid and dashed lines, respectively. (bottom) The magnetically conjugate magnetospheric locations for the auroral currents.

to both  $\Phi_{||}$  and  $j_{||i}$ . As we do not self-consistently calculate  $\Phi_{||}$  in this study, it is difficult to estimate the precipitating auroral energy flux without making simplifying assumptions. In the limit of

$$1 \ll \frac{e\Phi_{||}}{T_e} \ll R_B \tag{21}$$

where  $R_B$  is the magnetic mirror ratio between the top of the acceleration region to the planetary atmosphere, the field-aligned current density can be simply related to the potential strength by

$$j_{||i} = \frac{e^2 n}{\sqrt{2\pi m_e T_e}} \Phi_{||} \tag{22}$$

The precipitating energy flux would then be given by  $EF = j_{||i} \Phi_{||}$ . At Jupiter, the latter inequality of equation (21) is likely not satisfied. However, there is still some insight to be gained from this simplified approximation. Figure 6 shows the estimated precipitating auroral energy flux from equation (22). Only energy fluxes greater than  $1 \text{ mW m}^{-2}$ , and therefore detectable by HST, are shown. As indicated by the auroral currents, the brightest emission occurs from 0500 LT to 0700 LT. There are two discontinuities, from 1300 to 1500LT and again from 1800 to 2000 LT. The predicted precipitating auroral electron energy fluxes are consistent with the range of  $2\text{--}30 \text{ mW m}^{-2}$  derived from HST observations [Gustin *et al.*, 2004]; however, the estimate does ignore the location of the acceleration region and the rotational decoupling related to perpendicular gradients in the field-aligned potential strength and should be taken as a rough value or “order-of-magnitude” estimate.

#### 4. Conclusions

We present a simplified 1-D model of variations in the auroral currents coupling Jupiter’s magnetosphere and ionosphere. Using a local time dependent equatorial magnetic field structure [Vogt *et al.*, 2011] and flux

Smith and Aylward [2009] coupled a model of the auroral currents to a general circulation model of Jupiter’s atmosphere. They found that including thermospheric feedback kept the plasma angular velocity nearer to corotation in the inner magnetosphere. Again, this points to our predicted plasma angular velocities being underestimates.

Finally, the development of high-latitude field-aligned potentials and their decoupling effects are ignored in this study. Ray *et al.* [2010] found that the interplay between the rotational decoupling allowed by field-aligned potentials and enhancements in the Pedersen conductance led to slightly enhanced plasma angular velocities relative to the case of a variable  $\Sigma_p$  and equipotential field lines. They also found the peak intensity of the ionospheric field-aligned current density to be smaller than those predicted by models assuming equipotential field lines [e.g., Nichols and Cowley, 2004], albeit broader in latitude. The benefit to this approach is that the auroral energy flux can be explicitly calculated as it is related

function, we apply our 1-D model every hour in local time or, equivalently, every 15° in inertial longitude to investigate how variations in the magnetospheric magnetic field affect the plasma angular velocity profile, and the location and magnitude of the auroral currents. We find that

1. Auroral currents are strongest in the dawn region from 0500 LT to 0700 LT, surpassing those in the noon through dusk region by an order of magnitude or more.
2. In the dawn region, the corotation enforcement currents driving the main auroral emission extend to the magnetosphere boundary.
3. The stronger magnitude of  $B_N$  through noon and dusk, relative to dawn, leads to smaller radial, and, by extension, field-aligned currents as the current contribution to the  $\mathbf{J} \times \mathbf{B}$  force becomes less necessary to maintain plasma corotation. Consequently, in this model the noon through dusk regions are associated with dim auroral emission, with possible discontinuities in the oval.
4. Through noon and dusk, the maximum height-integrated radial current running through the magnetosphere is less than half that at dawn.
5. The trends in the azimuthal velocity of the plasma predicted by our 1-D model are opposite to those observed by the Galileo EPD. This is likely due to the assumption of azimuthal symmetry, which underlies the 1-D model.

Future studies of local time variation in the M-I current system should consider the bendback of the planetary magnetic field. The predicted minimums in the auroral and radial currents in this model are shifted toward dusk from the observed auroral observations and measured magnetospheric currents. As such, this simplified 1-D approach needs to be improved before it can be coupled to more sophisticated models of M-I coupling, which would include thermospheric feedback, variable Pedersen conductances, and the development of high-latitude field-aligned potentials. How best to implement azimuthal variations in an M-I coupling study is an important area for future research.

#### Acknowledgments

L.C.R. was supported by NSF grant 1064635 and would also like to acknowledge the ISSI team on Comparative Jovian Aeronomy for useful conversations. N.A. was supported by STFC's UCL Astrophysics Consolidated grant ST/J001511/1. The authors acknowledge support of computational resources provided as part of the STFC-funded Miracle project (now completed). M.F.V. was supported by STFC's Consolidated grant ST/K001000/1. J.N.Y. was supported by STFC's Imperial College Astrophysics and Space Physics Consolidated grant ST/K001051/1. The models used in this research will be made available upon request by L.C.R. The authors thank the referees for useful comments and suggestions that improved the quality of the manuscript.

Michael Liemohn thanks Jerry Goldstein and another reviewer for their assistance in evaluating this paper.

#### References

- Branduardi-Raymont, G., R. F. Elsner, M. Galand, D. Grodent, T. E. Cravens, P. Ford, G. R. Gladstone, and J. H. Waite (2008), Spectral morphology of the X-ray emission from Jupiter's aurorae, *J. Geophys. Res.*, *113*, A02202, doi:10.1029/2007JA012600.
- Chané, E., J. Saur, and S. Poedts (2013), Modeling Jupiter's magnetosphere: Influence of the internal sources, *J. Geophys. Res. Space Physics*, *118*, 2157–2172, doi:10.1002/jgra.50258.
- Clarke, J. T., L. Ben Jaffel, and J.-C. Gérard (1998), Hubble Space Telescope imaging of Jupiter's UV aurora during the Galileo orbiter mission, *J. Geophys. Res.*, *103*, 20,217–20,236, doi:10.1029/98JE01130.
- Clarke, J. T., D. Grodent, S. W. H. Cowley, E. J. Bunce, P. Zarka, J. E. P. Connerney, and T. Satoh (2004), Jupiter's aurora, in *Jupiter. The Planet, Satellites and Magnetosphere*, edited by F. Bagenal, T. E. Dowling, and W. B. McKinnon, pp. 639–670, Cambridge Univ. Press, Cambridge, U. K.
- Cowley, S. W. H., and E. J. Bunce (2001), Origin of the main auroral oval in Jupiter's coupled magnetosphere-ionosphere system, *Planet. Space Sci.*, *49*, 1067–1088.
- Cowley, S. W. H., and E. J. Bunce (2003), Corotation-driven magnetosphere-ionosphere coupling currents in Saturn's magnetosphere and their relation to the auroras, *Ann. Geophys.*, *21*, 1691–1707, doi:10.5194/angeo-21-1691-2003.
- Delamere, P. A., F. Bagenal, and A. Steffl (2005), Radial variations in the Io plasma torus during the Cassini era, *J. Geophys. Res.*, *110*, A12223, doi:10.1029/2005JA011251.
- Gérard, J.-C., D. Grodent, A. Radioti, B. Bonfond, and J. T. Clarke (2013), Hubble observations of Jupiter's north-south conjugate ultraviolet aurora, *Icarus*, *226*, 1559–1567, doi:10.1016/j.icarus.2013.08.017.
- Grodent, D., J. T. Clarke, J. Kim, J. H. Waite, and S. W. H. Cowley (2003), Jupiter's main auroral oval observed with HST-STIS, *J. Geophys. Res.*, *108*, 1389, doi:10.1029/2003JA009921.
- Grodent, D., J. Gérard, A. Radioti, B. Bonfond, and A. Saglam (2008a), Jupiter's changing auroral location, *J. Geophys. Res.*, *113*, A01206, doi:10.1029/2007JA012601.
- Grodent, D., B. Bonfond, J.-C. Gérard, A. Radioti, J. Gustin, J. T. Clarke, J. Nichols, and J. E. P. Connerney (2008b), Auroral evidence of a localized magnetic anomaly in Jupiter's northern hemisphere, *J. Geophys. Res.*, *113*, A09201, doi:10.1029/2008JA013185.
- Gustin, J., J.-C. Gérard, D. Grodent, S. W. H. Cowley, J. T. Clarke, and A. Grard (2004), Energy-flux relationship in the FUV Jovian aurora deduced from HST-STIS spectral observations, *J. Geophys. Res.*, *109*, A10205, doi:10.1029/2003JA010365.
- Gustin, J., S. W. H. Cowley, J.-C. Gérard, G. R. Gladstone, D. Grodent, and J. T. Clarke (2006), Characteristics of Jovian morning bright FUV aurora from Hubble Space Telescope/Space Telescope Imaging Spectrograph imaging and spectral observations, *J. Geophys. Res.*, *111*, A09220, doi:10.1029/2006JA011730.
- Hill, T. W. (1979), Inertial limit on corotation, *J. Geophys. Res.*, *84*, 6554–6558.
- Hill, T. W. (2001), The Jovian auroral oval, *J. Geophys. Res.*, *106*, 8101–8108, doi:10.1029/2000JA000302.
- Huang, T. S., and T. W. Hill (1989), Corotation lag of the Jovian atmosphere, ionosphere, and magnetosphere, *J. Geophys. Res.*, *94*, 3761–3765.
- Joy, S. P., M. G. Kivelson, R. J. Walker, K. K. Khurana, C. T. Russell, and T. Ogino (2002), Probabilistic models of the Jovian magnetopause and bow shock locations, *J. Geophys. Res.*, *107*, 1309, doi:10.1029/2001JA009146.
- Khurana, K. K. (2001), Influence of solar wind on Jupiter's magnetosphere deduced from currents in the equatorial plane, *J. Geophys. Res.*, *106*, 25,999–26,016, doi:10.1029/2000JA000352.
- Khurana, K. K., and H. K. Schwarzl (2005), Global structure of Jupiter's magnetospheric current sheet, *J. Geophys. Res.*, *110*, A07227, doi:10.1029/2004JA010757.

- Khurana, K. K., M. G. Kivelson, V. M. Vasyliunas, N. Krupp, J. Woch, A. Lagg, B. H. Mauk, and W. S. Kurth (2004), The configuration of Jupiter's magnetosphere, in *Jupiter. The Planet, Satellites and Magnetosphere*, edited by F. Bagenal, T. E. Dowling, and W. B. McKinnon, pp. 593–616, Cambridge Univ. Press, Cambridge, U. K.
- Kivelson, M. G., and K. K. Khurana (2002), Properties of the magnetic field in the Jovian magnetotail, *J. Geophys. Res.*, *107*(A8), 1196, doi:10.1029/2001JA000249.
- Kivelson, M. G., and D. J. Southwood (2005), Dynamical consequences of two modes of centrifugal instability in Jupiter's outer magnetosphere, *J. Geophys. Res.*, *110*, A12209, doi:10.1029/2005JA011176.
- Krupp, N., A. Lagg, S. Livi, B. Wilken, J. Woch, E. C. Roelof, and D. J. Williams (2001), Global flows of energetic ions in Jupiter's equatorial plane: First-order approximation, *J. Geophys. Res.*, *106*, 26,017–26,032, doi:10.1029/2000JA900138.
- Melin, H., S. Miller, T. Stallard, C. Smith, and D. Grodent (2006), Estimated energy balance in the jovian upper atmosphere during an auroral heating event, *Icarus*, *181*, 256–265, doi:10.1016/j.icarus.2005.11.004.
- Millward, G., S. Miller, T. Stallard, A. D. Aylward, and N. Achilleos (2002), On the dynamics of the jovian ionosphere and thermosphere III. The modelling of auroral conductivity, *Icarus*, *160*, 95–107, doi:10.1006/icar.2002.6951.
- Nichols, J. D. (2011), Magnetosphere-ionosphere coupling currents in Jupiter's middle magnetosphere: Computations including a self-consistent current sheet magnetic field model, *J. Geophys. Res.*, *116*, A10232, doi:10.1029/2011JA016922.
- Nichols, J. D., and S. W. H. Cowley (2004), Magnetosphere-ionosphere coupling currents in Jupiter's middle magnetosphere: Effect of precipitation-induced enhancement of the ionospheric Pedersen conductivity, *Ann. Geophys.*, *22*, 1799–1827.
- Nichols, J. D., and S. W. H. Cowley (2005), Magnetosphere-ionosphere coupling currents in Jupiter's middle magnetosphere: Effect of magnetosphere-ionosphere decoupling by field-aligned auroral voltages, *Ann. Geophys.*, *23*, 799–808.
- Nichols, J. D., J. T. Clarke, J. C. Gérard, D. Grodent, and K. C. Hansen (2009), Variation of different components of Jupiter's auroral emission, *J. Geophys. Res.*, *114*, A06210, doi:10.1029/2009JA014051.
- Pontius, D. H. (1997), Radial mass transport and rotational dynamics, *J. Geophys. Res.*, *102*, 7137–7150, doi:10.1029/97JA00289.
- Radioti, A., J. Gérard, D. Grodent, B. Bonfond, N. Krupp, and J. Woch (2008), Discontinuity in Jupiter's main auroral oval, *J. Geophys. Res.*, *113*, A01215, doi:10.1029/2007JA012610.
- Ray, L. C., Y. Su, R. E. Ergun, P. A. Delamere, and F. Bagenal (2009), Current-voltage relation of a centrifugally confined plasma, *J. Geophys. Res.*, *114*, A04214, doi:10.1029/2008JA013969.
- Ray, L. C., R. E. Ergun, P. A. Delamere, and F. Bagenal (2010), Magnetosphere-ionosphere coupling at Jupiter: Effect of field-aligned potentials on angular momentum transport, *J. Geophys. Res.*, *115*, A09211, doi:10.1029/2010JA015423.
- Ray, L. C., R. E. Ergun, P. A. Delamere, and F. Bagenal (2012), Magnetosphere-ionosphere coupling at Jupiter: A parameter space study, *J. Geophys. Res.*, *117*, A01205, doi:10.1029/2011JA016899.
- Scudder, J. D., E. C. Sittler, and H. S. Bridge (1981), A survey of the plasma electron environment of Jupiter: A view from Voyager, *J. Geophys. Res.*, *86*, 8157–8179.
- Smith, C. G. A., and A. D. Aylward (2009), Coupled rotational dynamics of Jupiter's thermosphere and magnetosphere, *Ann. Geophys.*, *27*, 199–230.
- Stallard, T., S. Miller, G. Millward, and R. D. Joseph (2001), On the dynamics of the jovian ionosphere and thermosphere. I. The measurement of ion winds, *Icarus*, *154*, 475–491, doi:10.1006/icar.2001.6681.
- Su, Y., R. E. Ergun, F. Bagenal, and P. A. Delamere (2003), Io-related Jovian auroral arcs: Modeling parallel electric fields, *J. Geophys. Res.*, *108*(A2), 1094, doi:10.1029/2002JA009247.
- Tao, C., H. Fujiwara, and Y. Kasaba (2009), Neutral wind control of the Jovian magnetosphere-ionosphere current system, *J. Geophys. Res.*, *114*, A08307, doi:10.1029/2008JA013966.
- Tao, C., H. Fujiwara, and Y. Kasaba (2010), Jovian magnetosphere-ionosphere current system characterized by diurnal variation of ionospheric conductance, *Planet. Space Sci.*, *58*, 351–364, doi:10.1016/j.pss.2009.10.005.
- Vasavada, A. R., A. H. Bouchez, A. P. Ingersoll, B. Little, C. D. Anger, and Galileo SSI Team (1999), Jupiter's visible aurora and Io footprint, *J. Geophys. Res.*, *104*, 27,133–27,142, doi:10.1029/1999JE001055.
- Vogt, M. F., M. G. Kivelson, K. K. Khurana, R. J. Walker, B. Bonfond, D. Grodent, and A. Radioti (2011), Improved mapping of Jupiter's auroral features to magnetospheric sources, *J. Geophys. Res.*, *116*, A03220, doi:10.1029/2010JA016148.
- Walker, R. J., and T. Ogino (2003), A simulation study of currents in the Jovian magnetosphere, *Planet. Space Sci.*, *51*, 295–307, doi:10.1016/S0032-0633(03)00018-7.
- Yates, J. N., N. Achilleos, and P. Guio (2012), Influence of upstream solar wind on thermospheric flows at Jupiter, *Planet. Space Sci.*, *61*, 15–31, doi:10.1016/j.pss.2011.08.007.
- Yates, J. N., N. Achilleos, and P. Guio (2014), Response of the Jovian thermosphere to a transient 'pulse' in solar wind pressure, *Planet. Space Sci.*, *91*, 27–44, doi:10.1016/j.pss.2013.11.009.